A PIV STUDY OF FLUID FLOW THROUGH PARALLEL COMMUNICATING LAYERS OF POROUS MEDIA

James K Arthur, Douglas W. Ruth and Mark F. Tachie
University of Manitoba

This paper was prepared for presentation at the International Symposium of the Society of Core Analysts held in Abu Dhabi, UAE 29 October-2 November, 2008

ABSTRACT

The paper reports results of a particle image velocimetry (PIV) study of the flow of water through layers of model parallel, communicating porous media when the layers have the same porosity and when the porosities of the layers differ. The model porous media is constructed of a square array of acrylic rods designed such that porosities of 0.99, 0.975, 0.95, 0.80, 0.78 and 0.51 are achieved. It is shown that flow in a free channel closely matches the expected, parabolic profile. For systems when a free zone is above a porous layer, it is shown that, even for modest values of porosity, the vast majority of the fluid flows through the free zone. If the system consists of only two porous layers (no free zone) of the same porosity, a very symmetrical flow pattern results. For systems consisting of a free zone between two porous zones of the same porosity, the free zone again carries most of the flow. If the two porous zones have different porosities, complicated flow patterns can result. However, for even modest porosity contrasts, the higher porosity zone carries the bulk of the flow. These results have direct application in engineering systems such as tube-in-shell heat exchangers. However, they also provide essential insights into reservoir processes such as flow in fractured reservoirs, and flow in parallel zones which communicate. The results demonstrate that, for even these simple systems, single phase flow patterns can become very complex.

INTRODUCTION

The study of flow through porous media has important engineering applications in areas such as water or hydrocarbon reservoirs, filters, and heat pipe technology. Although these flow applications may be shear-driven, multi-phase, and show the presence of inertial effects, the scope of this study is limited to that of pressure-driven single-phase flows, for which inertia is not a factor. Even in those limitations, the above-mentioned examples are still applicable. These flows are generally three-dimensional. Due to its practical importance, the study of flow phenomena through porous media has attracted considerable research interest. Reviews by Scheidegger (1974) provide much information about past research developments. Numerous theoretical and experimental studies have been made in both pressure and shear driven flows in which various geometries have been used to represent the real porous media (as reviewed by Larson and Higdon, 1986). Following previous works (*eg.* Agelinchaab *et al*, 2006), the present study uses a model porous medium, consisting of a square array of circular cylinders, shown in the representative sectioned top view of Figure 1(a). As schematized again in Figures 1(a) and (b),

respectively, flow through porous medium may be bounded by a free zone or by another porous medium so that the lower and upper porous media may be touching. These configurations pertain to applications such as reservoirs made up of adjoining layers of rocks of equal or unequal porosity. In fractured reservoirs for example, the lower and upper porous surfaces may be of equal or different porosities with a free zone between the media. This is the condition shown in Figure 1(c). A typical velocity distribution, $U(Y)$ for a pressure-driven flow is shown in Figure 1(a). In any given case however, the flow inside the porous medium, if sufficiently slow is considered to be governed by Darcy's law, equivalently stated (Gupte and Advani, 1997) as:

$$\nabla p = -\frac{\mu \cdot U}{k} \tag{1}$$

where ∇p is the applied pressure gradient, μ is the fluid dynamic viscosity and U is the mean filter velocity. For a model porous medium of long circular cylinders with uniform diameter, the specific Darcy permeability k may be calculated in terms of porosity, ϕ by the following relation (Jackson & James, 1986):

$$\frac{k}{r^2} = \frac{1}{8(1-\phi)}\left[-\ln(1-\phi) - 1.476 + 2(1-\phi) - 1.774(1-\phi)^2 + 4.076(1-\phi)^3\right] \tag{2}$$

where r is the radius of the cylinder cross section. Although fluid flow through and over a porous medium has been studied extensively, prior investigations have been dominated by either shear-flow or two-dimensional pressure-driven cases (e.g. Tachie *et al*, 2002, 2003; Gupte and Advane, 1997). Such flows are usually bounded by a free zone. The literature provides only theoretical solutions of simplified two-dimensional flow at the interface of two porous media (Vafai and Thiyagaraja, 1987), but no detailed experimental reports for three-dimensional flow through and over a porous medium bounded by another porous medium. As a result, many questions about the flow phenomenon, such as modes of communication between adjoining layers of porous media of the same porosity or of different porosities remain unresolved. Furthermore, the general distributions of flow through layers of porous media separated by a free zone, are still unknown. The present study therefore seeks to provide some insight to the questions for the above-mentioned porous media flow boundary conditions. This is achieved by means of detailed PIV measurements of a pressure driven flow through and over model porous media covering a wide range of porosity ($0.51 \leq \phi \leq 0.99$).

EXPERIMENTAL APPARATUS AND MEASUREMENT PROCEDURE

Test Section and Porous Media Models

As schematized in Figure 1, the test channel was of length, L = 600 mm, width, W = 71 mm and of a depth, H. The depth could be varied by placing machined plates of specific thicknesses on the bottom surface. To enhance optical access, the test section and porous media models were constructed from transparent acrylic material, of refractive index 1.47. The porous media models were constructed by inserting circular rods into holes drilled into the plates. The rods were arranged in square arrays to obtain porosities of $0.51 \leq \phi \leq$

0.99. For a given rod diameter d, and ϕ, the spacing between rods l was determined from the relation: $l = d/2\sqrt{[\pi/(1-\phi)]}$.

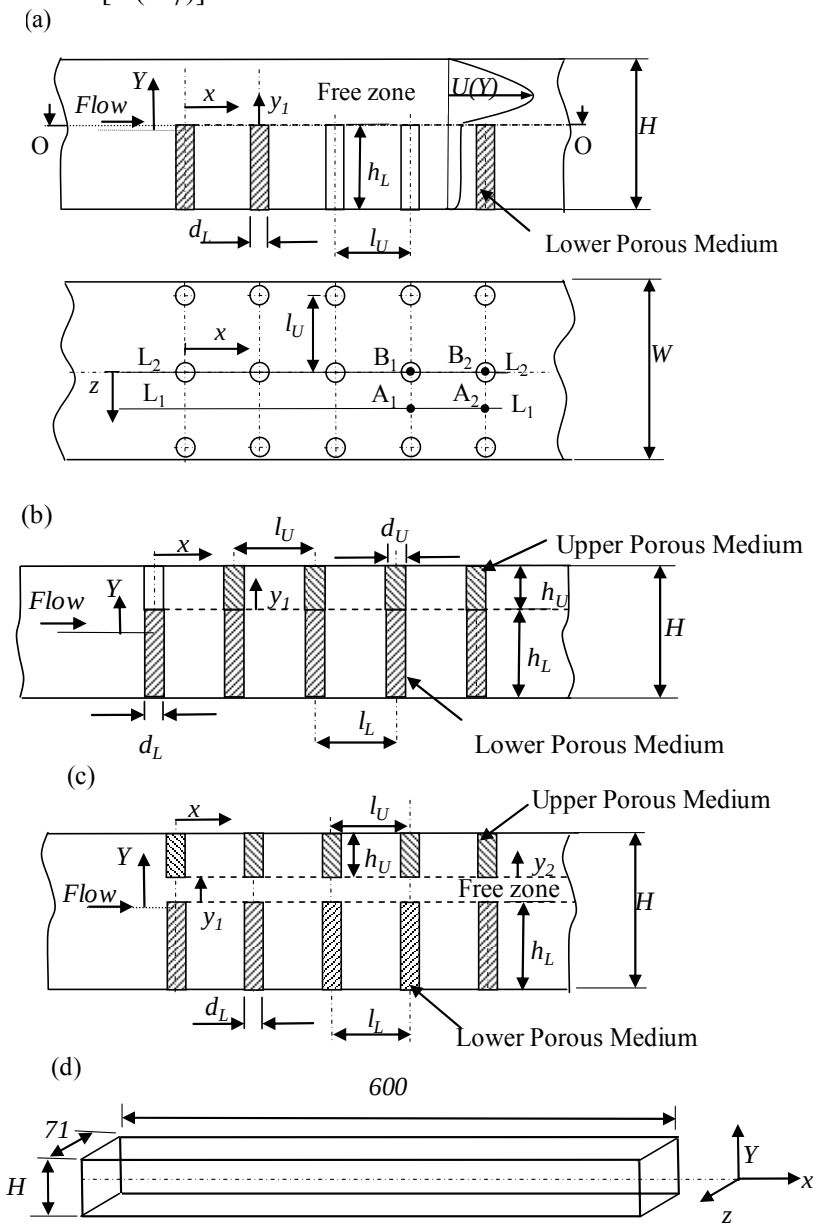

Figure 1: Schematic front view of flow through a model porous medium: (a) bounded by a free zone (in a pressure-driven flow), with a representative sectioned (O-O) top view; (b) bounded by another porous medium, with both media touching; (c) bounded by another porous medium, but with a free zone between the porous media. In (b) and (c), porosities in lower and upper media may be equal or unequal. (d) Test channel.

All numeric dimensions are in millimetres. Dashed lines represent interfaces between various sections porous medium and free zone or another porous medium.
Three diameters, d = 1.59 mm, 3.18 mm, and 4.76 mm, and three spacings between adjacent rods, l = 6.03 mm, 8.90 mm and 12.60 mm, were used. Each porous medium had at least six rods along the direction of flow. This was done to ensure that the flow inside the model porous medium developed to become periodic. The arrangement of rods also spanned the entire width of the channel. The center of the most upstream columns of rods was located 400 mm downstream from the inlet of the test section. Porous media rods of mean heights, h_L = 14 mm and h_U = 7 mm were used for the lower and upper channel walls.

As shown in Figure 1, the streamwise, transverse and spanwise directions are respectively denoted by x, y (or Y) and z. The location $x = 0$ coincides with the center of the most upstream columns of rods. For the transverse direction $y_1 = 0$ is at the interface between the lower porous medium and a free zone (as in Figure 1a); $y_2 = 0$ is also the interface between the upper porous medium and a free zone (as in Figure 1c); $Y = 0$ is the center-line between the lower and upper walls. The location, $z = 0$ is fixed at the channel mid-span.

The PIV System

The PIV and channel arrangement are shown in Figure 2. Water of kinematic viscosity $\nu = 1 \times 10^{-6}$ m^2/s, density $\rho = 1000$ kg/m^3, and a refractive index of 1.33, was used as the working fluid. A centrifugal pump supplied by Cole-Parmer Instruments Company and of maximum flow rate, 530.4 cm^3/s was used to deliver a non-pulsating low pressure flow into the channel. The flow was seeded using fluorescent polymer micro-sphere particles supplied by Duke Scientific Corporation with mean diameter and specific gravity, 6 μm and 1.05 respectively. A Nd-YAG, 120 mJ/pulse laser and 532 nm wavelength was used to illuminate the flow field. A set of cylindrical lens was used to convert the laser light into a thin sheet. The laser sheet was positioned in such a way that its plane was perpendicular to the camera. The seeding particles absorb and emit light at a wavelength of 542 nm and 612 nm, respectively. Since the particle settling velocity and response time, estimated to be 1.34 μm/s and 37.4 ps respectively, are very small compared with typical velocity and time scales of the flow, the particles were considered to follow the fluid faithfully. A C–mount 58 mm – 62 mm diameter EX Sigma lens, equipped with a band-pass filter was fitted to a Dantec Dynamic HiSense 4M digital camera using a charged-couple device (CCD). The CCD camera, of 2048 pixel × 2048 pixel chip, and pitch 7.4 μm, was used to capture images of the flow field. To minimize errors due to peak-locking while optimizing background contrast and resolution, a focal length of 11 and field of view, 46.5 mm × 46.5 mm was used in the measurement process. Each image was subdivided into 32 × 32 pixels and processed with 50% overlap to give a spatial resolution of 0.36 mm by 0.36 mm interrogation area (IA). During the image acquisition, the times between the pulses of laser were chosen so that the maximum particle displacement in an IA was less than 1/4 of the side of the IA. The images were stored continuously through a buffer system onto a desktop computer. The digital images were post-processed using the

adaptive-correlation option of FlowManager 4.50.17, commercial software developed by Dantec Dynamics.

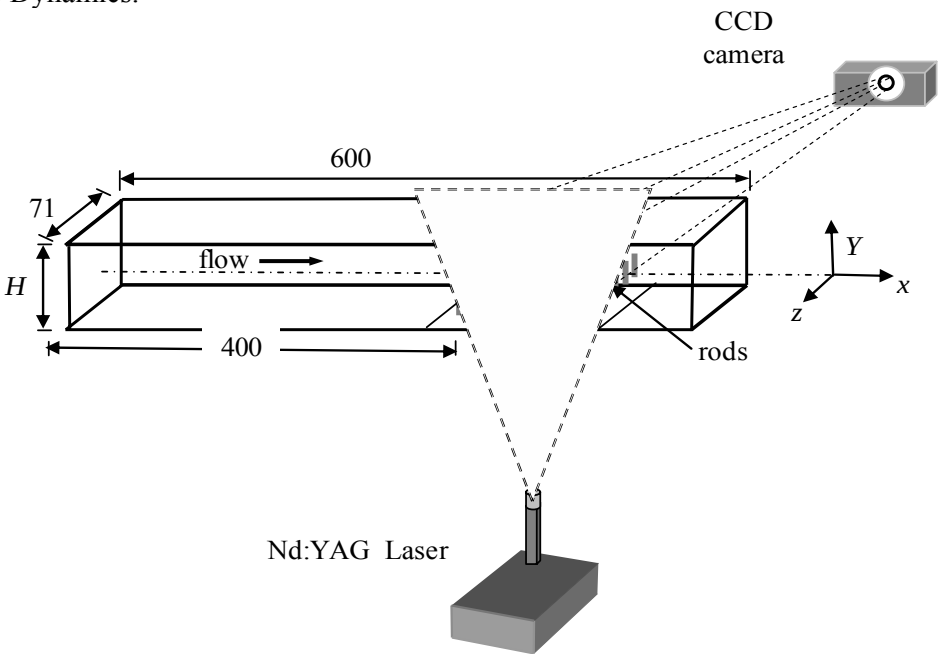

Figure 2: Schematic of channel and PIV setup. All numeric dimensions are in millimetres.

To account for the expected variations in flow along the channel span, extensive measurements were conducted in the x-y plane at z/l = 0, and 0.5 locations inside the porous medium and free zone. For the case of a pair of porous media of unequal ϕ on the channel walls, the measurements were made at the two z locations using the porous media of higher ϕ as the reference and for clarity, referred to as: $z/l_{H\phi}$ = 0, and 0.5. For the present experiments, the plane z/l or $z/l_{H\phi}$ = 0 passes between adjacent rows of the porous media rods of ϕ = 0.90, 0.95, 0.975, and 0.99. The plane z/l or $z/l_{H\phi}$ = 0.5 passes through the porous media rods of these models. On the other hand, due to the arrangement of porous media rods of ϕ = 0.78 and 0.51, the plane z/l = 0 or $z/l_{H\phi}$ = 0 rather passes through the rods whilst the z/l = 0.5 or $z/l_{H\phi}$ = 0.5 plane passes between adjacent rows of the rods. The plane passing between rods and that passing through rods are illustrated schematically in Figure 1(a) as L_1-L_1 and L_2-L_2, respectively, in the representative top view of a porous medium model. For convenience, these planes of measurement are hereafter referred to as PBR and PTR, respectively. Velocity data sets were line-averaged using a MATLAB script developed in our laboratory. With reference to Figure 1(a), velocity vectors taken in the PBR were typically line-averaged from rod centre A_1 to A_2, and in the PTR, from rod centre B_1 to B_2.

Preliminary Experiments, Measurement Uncertainties and Test Conditions

To determine the sample size N, necessary to achieve statistical convergence, measurements were made for flow in the channel without the porous medium present. The ensembled average streamwise velocity, u was then evaluated using different sample

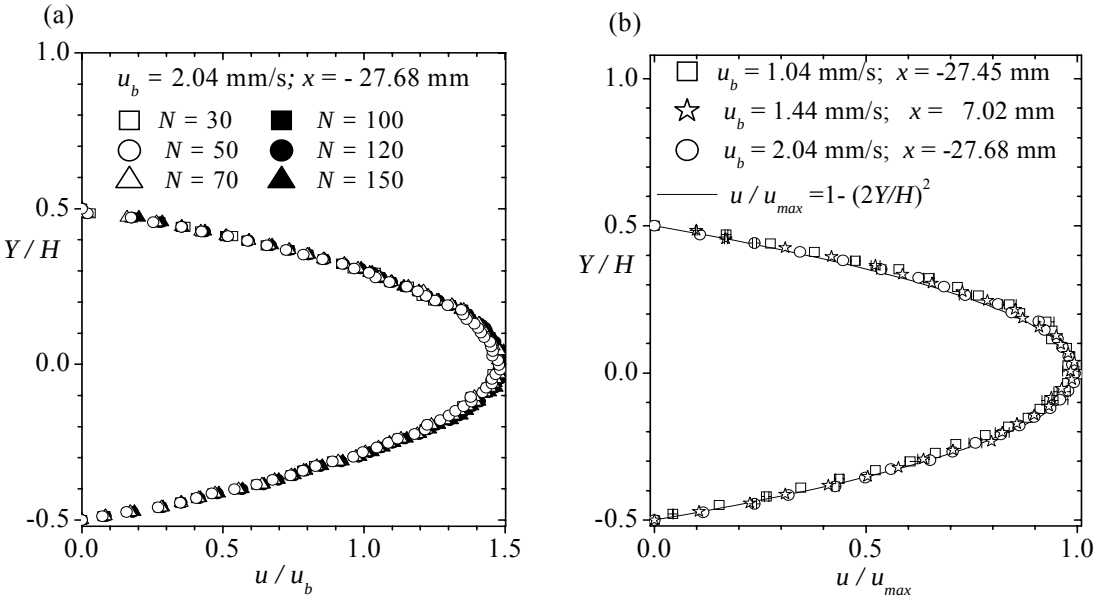

Figure 3: For a channel without porous medium: (a) results of convergence test are shown; and (b) profiles for flow at $z/l = 0$ are compared with the analytical profile.

sizes in the range $30 \leq N \leq 150$. The results in Figure 3 indicate that within the sample range used, the velocity profiles were independent of the sample size. A minimum sample size of 30 images was therefore used in subsequent measurements. In Figure 3 the transverse distance is normalized by the H. The velocities in Figure 3(a) are also normalized by the respective u_b. The profiles were parabolic, and as expected, the ratio of the centre line velocity to u_b was 1.5 in each case. To ascertain the accuracy of the velocities obtained from the PIV, velocity profiles obtained at different bulk velocities and streamwise locations were compared with analytically derived results. The velocity u was normalized by the corresponding local maximum velocity, u_{max}. As demonstrated in Figure 3(b), the measured profiles are in good agreement with the analytical profile, indicating a fully developed flow in the empty channel at the location of the porous media (*i.e.*, $x \geq 0$).

With the installation of the model porous media in the channel, the flow in the test section became three-dimensional. It is expected that the flow through the porous medium in the x direction would become periodic after a number of rows. To determine the region of periodicity, measurements were made in the x-y plane at $z/l = 0$, 0.5. The results show that the flow generally became periodic at $x/l \geq 2$ (*i.e.*, from the 3rd row onwards). For clarity, this trend is shown in Figure 4(a) extracted along the stream at a transverse location within the porous medium in the case of $\phi = 0.90$. All subsequent measurements were therefore taken at $x/l > 2$ to ensure that analysis was done only in the region of periodicity.

Another issue of concern was that of inertia. Equation (1) is valid in sufficiently low Reynolds number regimes. The global Reynolds number in this work is defined as

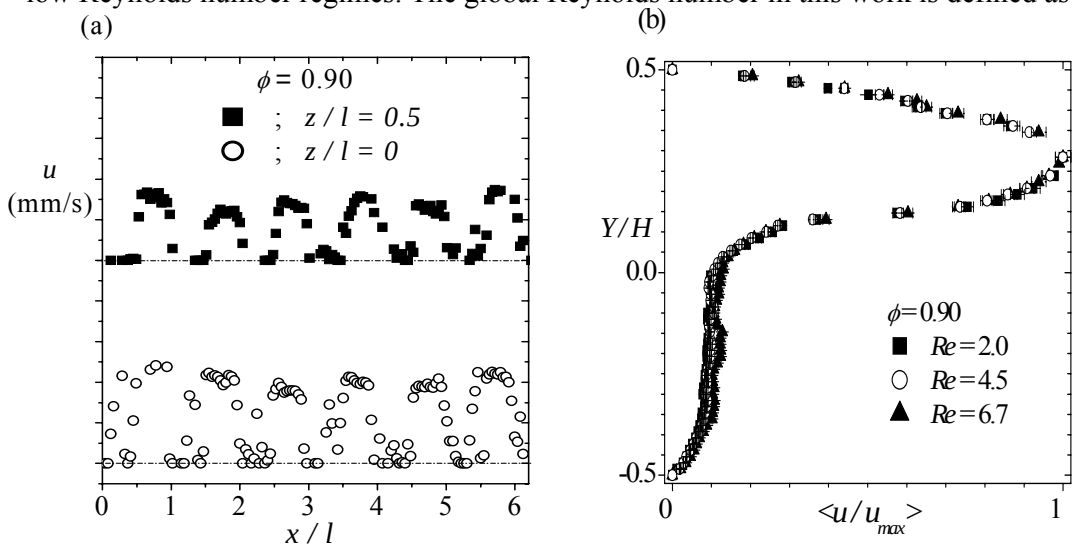

Figure 4: (a) Streamwise velocity profile at a selected *y* location to demonstrate porous media flow development (b) Demonstration of negligible *Re* effect on the flow through channel of with model porous medium on bottom wall of $\phi = 0.90$.

$Re = \langle u_b \rangle d/\nu$ (where $\langle u_b \rangle$ is the bulk of the line-averaged streamwise velocities). It should be noted that the Reynolds number in prior investigation (*e.g.* Agelinchaab *et al*, 2005) have been at most 1. Initial tests conducted with the pump showed that at very low flow rates (*i.e.*, $u_b < 1$ mm/s for $H = 25$ mm in a channel flow with no porous media present), there tended to be regions of back-flow. This resulted in sinusoidal mean velocity profiles even at the region of fully developed flow in the channel. For rods of minimum diameter, $d = 1.59$ mm, and the working fluid being water of kinematic viscosity $\nu = 1 \times 10^{-6}$ m^2/s at 20ºC, it was evident that the present test conditions would yield $Re > 1$. A test of inertial effects was thus needed. To do this, velocity measurements were made for model porous media of $\phi = 0.025$ and 0.10 on the bottom wall only, and at various bulk velocities. This was done to cover $2.0 \leq Re \leq 6.7$. As shown in Figure 4(b), the line-averaged streamwise velocity, $\langle u \rangle$ is normalised by the corresponding maximum velocity $\langle u_{max} \rangle$. The data sets do collapse reasonably. Based on these results, it can be concluded that for the range of *Re* considered in this work, the effects of inertia are negligible.

To assess the measurement uncertainty in u, both bias and precision errors were identified and quantified in each aspect of the measurement chain as outlined by Coleman and Steele (1995). A number of precautionary measures (as already described in a previous section) were taken to minimize errors such as those due to peak-locking as well as particle response to fluid motion and light pulse timing. The values of the total uncertainty were typically found to be 2% and 1% of u inside the porous media and in the free zone, respectively.

Detailed measurements were made at the test conditions summarized in Table 1.

Table 1. Summary of test conditions for (a) 1st Series (b) 2nd Series, and (c) 3rd Series of experiments; h_L = 14 mm and h_U= 7 mm.

(a)

H (mm)	d_L (mm)	l_L (mm)	ϕ_L	$<u_b>$ (mm/s)	Re_L
25	1.59	12.60	0.99	0.71	1.1
25	1.59	8.90	0.975	0.55	0.9
25	3.18	12.60	0.95	0.66	2.1
25	3.18	8.90	0.90	0.59	1.9
25	3.18	6.03	0.78	0.56	1.8
25	4.76	6.03	0.51	0.60	2.9

(b)

H (mm)	d_L (mm)	d_U (mm)	l_L (mm)	l_U (mm)	ϕ_L	ϕ_U	$<u_b>$ (mm/s)	Re_L, Re_U
22	1.59	1.59	12.60	12.60	0.99	0.99	1.00	1.6
22	1.59	1.59	8.90	8.90	0.975	0.975	0.66	1.1
22	3.18	3.18	12.60	12.60	0.95	0.95	0.89	2.8
22	3.18	3.18	8.90	8.90	0.90	0.90	0.41	1.3
25	1.59	1.59	12.60	12.60	0.99	0.99	1.05	1.7
25	1.59	1.59	8.90	8.90	0.975	0.975	1.05	1.7
25	3.18	3.18	12.60	12.60	0.95	0.95	0.88	2.8
25	3.18	3.18	8.90	8.90	0.90	0.90	0.73	2.3
25	4.76	4.76	6.03	6.03	0.51	0.51	0.40	1.9

(c)

H (mm)	d_L (mm)	d_U (mm)	l_L (mm)	l_U (mm)	ϕ_L	ϕ_U	$<U_b>$ (mm/s)	Re_L	Re_U
22	3.18	1.59	12.60	12.60	0.95	0.99	0.87	2.8	1.4
22	3.18	3.18	8.90	6.03	0.95	0.78	0.74	2.3	2.4
22	3.18	4.76	12.60	6.03	0.95	0.51	0.95	3.0	4.5
22	3.18	1.59	6.03	12.60	0.78	0.99	0.68	2.2	1.1
22	3.18	3.18	6.03	12.60	0.78	0.95	0.53	1.7	1.7
25	3.18	3.18	8.90	6.03	0.95	0.78	0.10	0.3	0.3
25	3.18	4.76	12.60	6.03	0.95	0.49	0.73	2.3	3.5
25	3.18	3.18	6.03	12.60	0.78	0.95	0.46	1.5	1.5

As indicated, the experiments were conducted in three series. In Series 1, the model porous medium was installed on the lower wall of the channel only, with a free zone above the porous medium. H was kept constant at 25 mm, whilst ϕ was varied from 0.99 to 0.51. In Series 2, model porous media of equal ϕ were installed on the bottom and top walls. In Series 2 and 3, model porous media of equal and non-equal ϕ were respectively installed

on the lower and upper walls, with each series using channel depths, $H \approx 22$ mm and 25 mm. In the former depth, the porous media on both walls were just touching, while in the latter depth, there was a free zone between the lower and upper porous media.

In Table 1 (and in Figures 1a-c), the height, diameter, and length of the rods used to fabricate the model porous media on the lower wall are denoted by h_L , d_L and l_L while those on the upper wall are denoted by h_U , d_U and l_U. The porosities of the model porous media on the lower and upper walls are denoted by ϕ_L and ϕ_U, respectively. Re_L and Re_U are the characteristic global Reynolds number defined as $Re_L = <u_b> d_L/ \nu$ and $Re_U = <u_b> d_U/ \nu$. The bulk line-averaged velocity $<u_b>$ for a given condition was typically found to be of the same order of magnitude for the two planes of measurement. Only values of $<u_b>$ and the corresponding Re values in the planes z/l, $z/l_{H\phi} = 0$ are thus shown in Table 1. The Reynolds number Re was kept sufficiently low (i.e $Re < 4$) so that inertia was not a factor in the flow, as concluded from Figure 4(b).

RESULTS AND DISCUSSION

With regards to trends in velocities, similar observations were obtained for PBR and PTR, and related $z/l_{H\phi} = 0$, 0.5 planes in all boundary conditions. Only PBR and $z/l_{H\phi} = 0$ velocity measurements are reported in this paper. The reader may refer to Arthur (2008) for the plane profiles omitted, and for a more detailed discussion. In the profiles presented in Figure 5, line-averaged velocities, $<u>$ are normalized by the local bulk velocity of the flow $<u_{b,}>$ (with the porous media present). The transverse distance has been normalized by the respective channel depth, H. Percentage flow rate distributions per unit span of the channel for flow through the relevant porous media and free zone for the various boundary conditions are also given in Table 2. In that table the permeability k for each porous medium has been computed from Equation (2). The subscripts L and U are used to represent lower and upper permeability values in k_L and k_U respectively.

In Figure 5(a), the profiles for the case of a porous medium on the lower channel wall only, bounded by a free zone, is shown. It is observed that the porous medium on the lower wall of the channel blocks the flow within the porous medium. From Table 2, it is noted that the extent of flow blockage is significant even at high ϕ so that at $\phi = 0.95$, flow into the porous medium is less than 40% of the bulk. This value generally reduces with decreasing ϕ so that $\phi = 0.78$ is just sufficient to allow no more than 1% flow inside the porous media.

Profiles for the case of porous media of touching porous media on lower and upper walls are shown in Figure 5(b). As given for $\phi_L = \phi_U = 0.95$ in Table 2, it is observed that for a pair of equal ϕ, the flow through the lower porous media is about 68% of the overall flow. This is expected since the depth filled by the lower porous medium is about 66% the total channel depth. The results for the case where $\phi_L \neq \phi_U$ show that the effect of varying the porosity from 0.78 to 0.51 is insignificant within experimental errors. In each of the cases for this boundary condition, it is found that there is greater flow in the porous medium with the lower ϕ independent of the fraction of the channel depth filled (filling fraction) by porous medium of larger ϕ.

A typical case is the combination of $\phi = 0.95$ and 0.78 where at least 96% of the

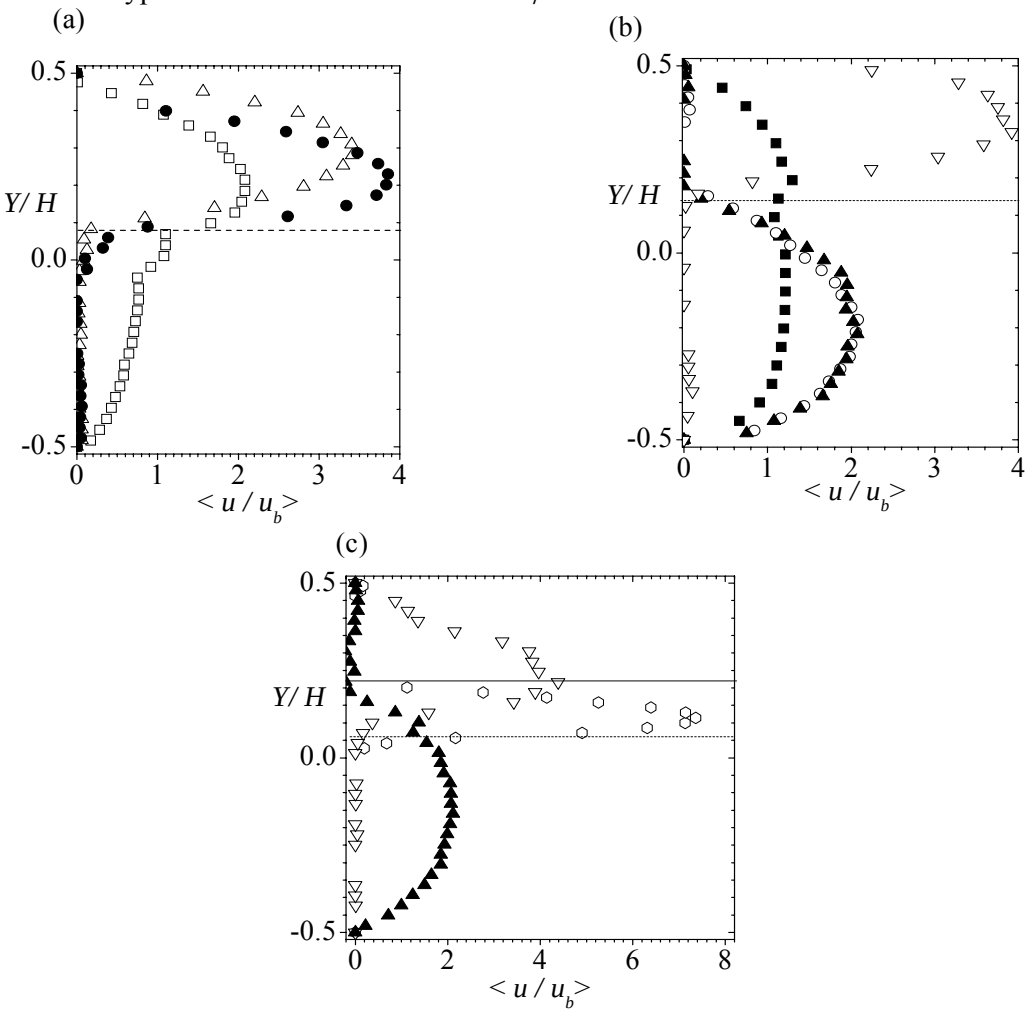

Figure 5: Bulk velocity distributions for: (a) Porous medium on lower channel wall only, bounded by a free zone (b) Porous medium on lower and upper channel walls, with both media touching (c) Porous media on both lower and upper channel walls, with the porous media not touching. Dashed and solid lines respectively show the lower and upper interfaces. The symbols used are: □ $\phi_L = 0.95, \phi_U$= plain wall ; ● $\phi_L = 0.78$, ϕ_U = plain wall; △ $\phi_L = 0.51$, ϕ_U= plain wall ; ■ $\phi_L = 0.95$, $\phi_U = 0.95$; ○ $\phi_L = 0.95$, $\phi_U = 0.51$; ▲ $\phi_L = 0.95$, $\phi_U = 0.78$; ▽ $\phi_L = 0.78$, $\phi_U = 0.95$; ⬡ $\phi_L = 0.51$, $\phi_U = 0.51$.

bulk flow is always in the porous medium of $\phi = 0.95$ regardless of the filling fraction occupied by a medium of this ϕ. The communication between adjoining layers of porous media in parallel flow is even more significant for $\phi_L = 0.95$. In that case, flow through the upper porous medium is increases considerably from less than 50% of the total flow rate to

about the total bulk flow, as ϕ_U is varied from 0.95 to 0.78. Compared with the flow bounded by the free zone, the observed flow distribution in the present boundary condition is similar since in both cases, the bulk flow is skewed towards the medium of higher ϕ.

Table 2: Summary results of percentage flow rate distributions for various boundary conditions of porous media flow in PBR and plane $z/l_{H\phi} = 0$. LPM – Lower Porous Medium; FZ – Free Zone; UPM – Upper Porous Medium; TPM – Touching Porous Media; NTPM – Non-Touching Porous Media.

Type	ϕ_L	ϕ_U	k_L (mm^2)	k_U (mm^2)	H (mm)	LPM (%)	FZ (%)	UPM (%)
LPM and FZ	0.95	-	10.20	-	25	38	62	-
	0.78	-	0.64	-	25	1	99	-
	0.51	0.95	0.39	10.20	25	0	100	-
TPM	0.95	0.95	10.20	10.20	22	68	-	32
	0.95	0.78	10.20	0.64	22	99	-	1
	0.95	0.51	10.20	0.39	22	98	-	2
	0.78	0.95	0.64	10.20	22	1	-	99
NTPM	0.51	0.51	0.39	0.39	25	21	77	2
	0.95	0.78	10.20	0.64	25	38	43	19
	0.78	0.95	0.64	10.20	25	0	36	64

For the porous medium flow bounded by another porous medium, but not touching each other, the flow is more complicated. At ϕ_L, $\phi_U = 0.51$, the flow rate is maximum in the free zone between the two media, where a clear parabolic profile is formed. This is shown in Figure 5(c) and quantified in Table 2. In this case, about 77% of the bulk flow is channelled into the free zone, so that flows within the lower and upper porous media were just about 21% and 2% respectively. This is of particular importance to fluid flow through fractured reservoirs. It is clear that the flow within each of the porous media cannot be considered separately as unidirectional parallel flows, with each described by (1). This is because such a treatment of the flow would suggest that the ratio of the flow rate distributions must then be comparable to the ratio of the permeability. However, a careful examination of results in Table 2 indicates that such an assumption does not hold, especially for flow through a pair of porous media with a free zone separating them. Furthermore, from the summary results of flow rate distributions, there seems to be other influences involved in the determination of the flow distributions. In the combination of $\phi = 0.78$ and 0.95, for example, there is significant filling fraction influence. When $\phi_L = 0.95$, the flow rate per unit span in the lower porous medium is 38% of the bulk, but when $\phi_L = 0.78$, the flow into the lower porous medium is stopped.

CONCLUSIONS

PIV velocity measurements of the flow of water through model porous medium bounded by a free zone, and layers of model parallel, communicating porous media equal and unequal porosities have been examined. Porosities of 0.99, 0.975, 0.95, 0.80, 0.78 and 0.51 were studied. For the case where a free zone is above a porous layer on the lower channel wall only, it is shown that even for 0.95 porosity, over 60% of the fluid flows through the free zone. If the system consists of only two porous layers of the same porosity, with the layers touching each other, the distributions through the porous media are predictable. For a low porosity system consisting of a free zone between two porous media of the same porosity, the free zone again carries most of the flow. However, if the two porous zones have different porosities, complicated flow patterns result, and even for modest porosity contrasts, the higher porosity zone carries the bulk of the flow. The implications of these results are of great value in the study of flow in fractured reservoirs, and flow in parallel zones which communicate. Furthermore, the results show that even for these simple models, single phase flow patterns can become very complex.

ACKNOWLEDGEMENTS

We gratefully acknowledge financial support of this work by the Natural Sciences and Engineering Research Council of Canada and Canada Foundation for Innovation through research grants to Drs D.W. Ruth and M.F. Tachie; and K. K. Adane for developing the MATLAB script used in the calculation of the line averages of the velocity data.

REFERENCES

1. Agelinchaab, M., Tachie, M.F. and Ruth, D.W. (2006) 'Velocity measurements of flow through a model three-dimensional porous medium,' Phys. Fluids. **1** Vol. **8**, pp 017105-1 – 11.
2. Arthur, J.K. (2008) 'Velocity measurements of flow through a model three-dimensional porous medium with varying boundary conditions,' Master of Science Thesis, University of Manitoba, Winnipeg, Manitoba.
3. Gupte, S. K. and Advani, S. G. (1997) 'Flow near the impermeable boundary of a porous medium: an experimental investigation using LDA,' Exp. Fluids. Vol. **22**, pp. 408 – 422.
4. Jackson, G. W. and James, D. F. (1986) 'The permeability of fibrous porous media,' Can. J. Chem. Eng. Vol. **64**, pp. 364 - 374.
5. Larson, R. E. and Higdon, J. J. L. (1986) 'Microscopic flow near the surface of two dimensional porous media. Part 1. Axial flow,' J. Fluid Mech. Vol. **166**, pp. 449–472.
6. Scheidegger, A. E., (1974) 'The physics of flow through porous media,' 3rd edn. University of Toronto Press.
7. Tachie, M.F., James, D. F., and Currie, I. G. (2003) 'Velocity measurements of the shear flow penetrating a porous medium,' J. Fluid Mech. Vol. **493**, pp. 319 – 343.
8. Tachie, M.F., James, D. F., and Currie, I. G. (2004) 'Slow flow through a brush,' Phys. Fluids. Vol. **16**, pp. 445-451.
9. Vafai, K. and Thyagaraja, R. (1987) 'Analysis of flow and heat transfer at the interface region of a porous medium,' Int. J. Heat Mass Transfer. Vol. **30**, pp. 1391 – 1405.